International Journal of Bifurcation and Chaos, Vol. 12, No. 8 (2002) 1843–1857

A NEW AND SIMPLE CHAOS TOY

ERIK M. BOLLT
Department of Mathematics and Computer Science, Clarkson University, Potsdam, NY 13699-5815, USA

AARON KLEBANOFF*
Mathematics Department, 572 Holloway Rd, U.S. Naval Academy, Annapolis, MD 21402-5002, USA

Received July 6, 2000; Revised April 6, 2002

We present two new, and perhaps the simplest yet, mechanical chaos demonstrations. They are both designed based on a recipe of competing nonlinear oscillations. One of these devices is simple enough that using the provided description, it can be built using a bicycle wheel, a piece of wood routed with an elliptical track, and a ball bearing. We provide a thorough Lagrangian mechanics based derivation of equations of motion, and a proof of chaos based on showing the existence of an embedded Smale horseshoe using Melnikov's method. We conclude with discussion of a future application.

Keywords: Melnikov function; chaos; KAM; Hamiltonian.

1. Introduction

Chaos theory has become a fundamental field in science and mathematics, which finds applications which run the gamut from physics, to chemistry, to biology, to medicine and to finance, just to get started. Yet, the number of simple and cheap-to-build mechanical demonstrations of the phenomenon of complex nonlinear oscillations is rather short. Many of us have a chaotic double pendulum [Shinbrot *et al.*, 1992; Rott, 1970] or perhaps the more messy Lorenz chaos waterwheel [Lorenz, 1993; Strogatz, 1994], but then the list of easy to build chaotic demonstrations [Moon, 1992] begins to run dry. It is our intention in this article to introduce a new variety of mechanical chaotic "toys", based on a principle of suspended but periodically forced systems. We will derive and analyze their dynamics, proving the existence of chaos by showing the existence of an embedded horseshoe, and also demonstrating important phenomenon including KAM-like invariant circles on a stroboscopic surface of section. Furthermore, we can arguably claim that our models are amongst the simplest mechanical chaotic toys possible in terms of their ease and cost to build. Nonetheless, we will discuss applications that such mechanical systems could serve with real engineering benefits.

We call the first model, "Elliptical Tube Toy", (ETT). We will build in steps the equations of motion for a ball-bearing rolling through a tube which has been bent into the shape of an ellipse, and the ellipse rotates about an axis through its center. See Fig. 1 and photograph Fig. 12. The unforced (not rotating) ellipse allows the ball-bearing to oscillate harmonically, but the rotation, in a rotating coordinate frame, appears as a periodically changing gravity field.

We call the second model, "Bouncing Tube Toy", (BTT). We will build, again in steps, the equations of motion for a ball-bearing rolling in

*Permanent Address: Mathematics Department CM 144, Rose-Hulman Institute of Technology, 5500 Wabash Avenue, Terre Haute, IN 47803, USA

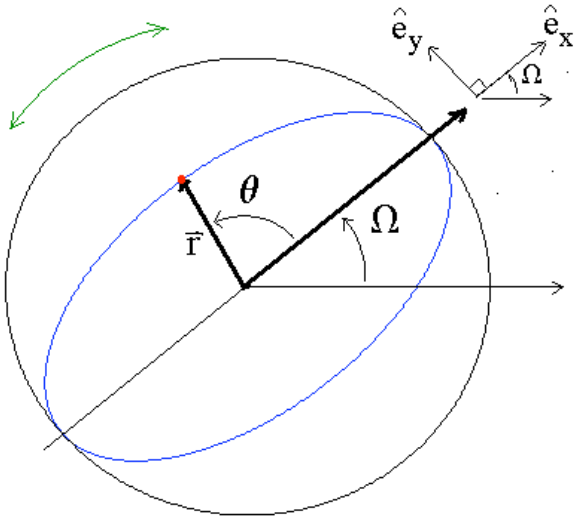

Fig. 1. Schematic drawing defining variables for a bead on a rotating ellipse.

a circular track, under the influence of an up and down periodic drive, which can be considered as a gravity of nonuniform magnitude. See Fig. 12.

A good rough rule which we had in mind when designing these chaotic systems is that an oscillator with its own intrinsic periods, which is externally forced by a competing force with comparable frequency, tends to not have the chance to fully recover, thus continually and wildly altering the motion. Both of the following models can be understood in this light. Furthermore, the periodic nature of the drive makes these systems especially amenable to a Melnikov analysis to prove the existence of an embedded horseshoe and therefore chaos, at least in the conservative models.

The ability to generate chaos in such a simple way has a practical engineering importance which we discuss in the conclusion as a topic for future research. In short, the area of chaos control has demonstrated that chaotic instability can be beneficial in that it allows the possibility that we might select and switch amongst the many different periodic motions embedded in an ergodic set [Ott *et al.*, 1990; Chen & Dong, 1998]. In the conclusion, we will mention that our mechanical chaotic devices have possible application to controlling chaotic oscillations of ship-to-ship transfers of cargo by shipboard cranes.

This paper is organized as follows. In Sec. 2, we introduce Model 1, the basic Elliptical Tube Toy Model (ETT), without rolling resistance, deriving the Hamiltonian equations of motion. In Sec. 3, we briefly review the Melnikov analysis and the resulting interpretations, and then we prove the existence of an embedded horseshoe in ETT. In Sec. 4, we present numerical results from ETT, showing the Poincaré maps for various parameter values, which demonstrate characteristic KAM-like invariant circles. We also show homoclinic tangles of stable and unstable manifolds promised by the Melnikov analysis, and that these are apparently still present beyond the parameter range allowed by the Melnikov analysis. In Sec. 5.1, we rederive the equations of motion for ETT, but this time in the presence of friction, in which case we discuss the fact the most invariant circles are destroyed, as are elliptic periodic cycles. In Sec. 5.2, we show that a fuller model of the physical ETT is easily derived, including rolling resistance and friction. In Sec. 6, we mention our cheaply and easily built physical model, based on a bicycle wheel, and we include a photograph. In Sec. 7, we introduce our second basic model, called Bouncing Tube Toy (BTT), and there we derive the Hamiltonian equations of motion and perform Melnikov analysis which again shows an embedded horseshoe. Also with BTT, we see the expected route to complexity of an area preserving map, in which successive invariant circles are destroyed as a control parameter is increased, progressively leading to a larger and connected chaotic set. Section 8 is the conclusion, in which we discuss the implications of our analysis, and we discuss possible engineering applications of Naval importance.

2. Model 1a: Elliptical Tube Toy (ETT) Without Rolling Resistance or Moment of Inertia

We now derive the most basic model for Elliptical Tube Toy (ETT). Without rolling resistance or moment of inertia, we essentially have a bead constrained to move on an elliptical wire without friction, and we will turn the ellipse uniformly. See Fig. 1. This bead-on-a-wire model is simple and a good model of a small moment of inertia ball-bearing. The full model with moment of inertia can be found in Sec. 5.2. See also our physical experiment shown in Fig. 12.

We follow the Lagrangian formulation to equations of motion.

Choosing a rotating coordinate frame to represent basis vectors, $\hat{\mathbf{e}}_\mathbf{x}$, and $\hat{\mathbf{e}}_\mathbf{y}$ at angle Ω, we

write,

$$\hat{\mathbf{e}}_{\mathbf{x}} = \begin{bmatrix} \cos(\Omega) & -\sin(\Omega) \\ \sin(\Omega) & \cos(\Omega) \end{bmatrix} \cdot \begin{bmatrix} 1 \\ 0 \end{bmatrix},$$
$$\text{and} \quad \hat{\mathbf{e}}_{\mathbf{y}} = \begin{bmatrix} \cos(\Omega) & -\sin(\Omega) \\ \sin(\Omega) & \cos(\Omega) \end{bmatrix} \cdot \begin{bmatrix} 0 \\ 1 \end{bmatrix}. \tag{1}$$

Now the bead on the wire is at time dependent position $\mathbf{r}(t)$,

$$\mathbf{r} = \cos(\theta)\hat{\mathbf{e}}_{\mathbf{x}} + b\,\sin(\theta)\hat{\mathbf{e}}_{\mathbf{y}}\,, \tag{2}$$

where $\theta(t)$ is a function of time, and we take the major axis of the ellipse to be $a = 1$, and the minor axis to be $b \leq 1$. Hence velocity is the derivative,

$$\begin{aligned} \mathbf{v} = &\left(-\sin(\theta)\dot{\theta}\hat{\mathbf{e}}_{\mathbf{x}} + \cos(\theta)\frac{d\hat{\mathbf{e}}_{\mathbf{x}}}{dt}\right) \\ &+ \left(b\,\cos(\theta)\dot{\theta}\hat{\mathbf{e}}_{\mathbf{y}} + b\,\sin(\theta)\frac{d\hat{\mathbf{e}}_{\mathbf{y}}}{dt}\right) \\ &\times(-\sin(\theta)\dot{\theta}\hat{\mathbf{e}}_{\mathbf{x}} + \cos(\theta)\dot{\Omega}\hat{\mathbf{e}}_{\mathbf{y}}) \\ &+ (b\,\cos(\theta)\dot{\theta}\hat{\mathbf{e}}_{\mathbf{y}} - b\,\sin(\theta)\dot{\Omega}\hat{\mathbf{e}}_{\mathbf{x}})\,, \end{aligned} \tag{3}$$

since $d[\hat{\mathbf{e}}_{\mathbf{x}}(\Omega)]/dt = \dot{\Omega}\hat{\mathbf{e}}_{\mathbf{y}}$, and likewise $d[\hat{\mathbf{e}}_{\mathbf{y}}(\Omega)]/dt = -\dot{\Omega}\hat{\mathbf{e}}_{\mathbf{x}}$.

From kinetic energy,

$$\begin{aligned} T = \frac{1}{2}m\mathbf{v}\cdot\mathbf{v} = \frac{1}{2}m[&\sin^2\theta(b\dot{\Omega} + \dot{\theta})^2 \\ &+ \cos^2\theta(b\dot{\theta} + \dot{\Omega})^2]\,, \end{aligned} \tag{4}$$

and potential energy,

$$U = mgh = mg[\sin\,\Omega\,\cos\,\theta + b\,\cos\,\Omega\,\sin\,\theta]\,, \tag{5}$$

follows the Lagrangian,

$$\begin{aligned} &L(\theta,\,\dot{\theta},\,t) \\ &\quad = T - U \\ &\quad = \frac{1}{2}m[\sin^2\theta(b\dot{\Omega} + \dot{\theta})^2 + \cos^2\theta(b\dot{\theta} + \dot{\Omega})^2] \\ &\qquad - mg[\sin\,\Omega\,\cos\,\theta + b\,\cos\,\Omega\,\sin\,\theta]\,. \end{aligned} \tag{6}$$

Now henceforth, we assume that the ellipse is subject to a uniform rotation,

$$\Omega(t) = \omega t + \omega_0\,, \tag{7}$$

and w.o.l.o.g. we choose $\omega_0 = 0$. The usual Lagrange equations of motion, $(d/dt)(\partial L/\partial\dot{\theta}) - (\partial L/\partial\theta) = 0$ give equations of motion in the form of a nonautonomous second-order differential equation.

We prefer here a Hamiltonian formulation [Goldstein, 1980; Abraham & Marsden, 1985], for the Melnikov analysis [Wiggins, 1990; Guckenheimer & Holmes, 1983] to follow. Canonical momentum is defined by,

$$p = \frac{\partial L}{\partial\dot{\theta}} = mb\omega + m\dot{q}(\sin^2 q + b^2\,\cos^2 q)\,, \tag{8}$$

where canonical position is the angle variable, $q \equiv \theta$. The Hamiltonian is derived by Legendre transformation,

$$\begin{aligned} &H(q,\,p,\,t) \\ &\quad = p\dot{q} - L(q,\,\dot{q},\,t) \\ &\quad = \frac{1}{2m}\frac{p^2}{\sin^2 q + b^2\cos^2 q} - \frac{b\omega p}{\sin^2 q + b^2\cos^2 q} \\ &\qquad + mg[\sin\,\omega t\,\cos\,q + b\,\cos\,\omega t\,\sin\,q] \\ &\qquad + \frac{1}{2}\frac{mb^2\omega^2}{\sin^2 q + b^2\cos^2 q} \\ &\qquad - \frac{1}{2}m\omega^2[\cos^2 q + b^2\sin^2 q]\,. \end{aligned} \tag{9}$$

From these follow the Hamiltonian equations of motion,

$$\begin{aligned} \frac{dq}{dt} &= \frac{p}{m(\sin^2 q + b^2\cos^2 q)} - \frac{b\omega}{\sin^2 q + b^2\cos^2 q} \\ \frac{dp}{dt} &= \frac{(b-1)(b+1)\sin(2q)(mb\omega - p)^2}{2m(\sin^2 q + b^2\cos^2 q)^2} \\ &\quad - \frac{1}{2}m\omega^2(1-b^2)\sin(2q) + mg(\sin(\omega t)\sin q \\ &\quad - b\,\cos(\omega t)\cos\,q) \end{aligned} \tag{10}$$

3. Horseshoe Chaos by Melnikov Function Analysis

We will show that the ETT Eqs. (10) display an embedded horseshoe set, on a stroboscopic surface of section, which is hence a chaotic set. Smale [1965] proved that a transverse homoclinic point of a hyperbolic periodic point $\mathbf{w}$ of a C^r diffeomorphism, $r \geq 2$, implies an embedded horseshoe. It is well

known and straightforward to prove that a horseshoe is chaotic. The Melnikov function gives a measure of the distance between stable and unstable manifolds, $W^s(\mathbf{w})$ and $W^u(\mathbf{w})$ with respect to a parameterization of these curves when this distance is small, and hence can be used to decide the existence of a transverse intersection [Wiggins, 1990].

We now describe the Melnikov analysis for an autonomous Hamiltonian system of the plane $\tilde{H}(q, p)$, under the influence of a small time periodic perturbation $g(q, p, t) = g(q, p, t + T)$ for some $T > 0$. The Melnikov analysis we use assumes a dynamical system of the form,

$$\frac{dq}{dt} = \frac{\partial \tilde{H}}{\partial p} + \varepsilon g_1(q, p, t) \tag{11}$$

$$\frac{dp}{dt} = -\frac{\partial \tilde{H}}{\partial q} + \varepsilon g_2(q, p, t)\,, \tag{12}$$

or $\dot{\mathbf{z}} = J \cdot \nabla \tilde{H}(\mathbf{z}) + \mathbf{g}(\mathbf{z}, t)$ where $J = \left(\begin{smallmatrix} 0 & 1 \\ -1 & 0 \end{smallmatrix}\right)$, $\nabla \tilde{H} = \langle (\partial \tilde{H}/\partial q), (\partial \tilde{H}/\partial p) \rangle^t$, $\mathbf{g} = \langle g_1, g_2 \rangle^t$, $\mathbf{z} = \langle q, p \rangle^t$, [Wiggins, 1990]. Furthermore, the unperturbed system $\dot{\mathbf{z}} = J \cdot \nabla \tilde{H}(\mathbf{z})$ must have a hyperbolic fixed point $\mathbf{w}$ with a homoclinic connection orbit, which we call $\mathbf{z}^*(t)$, which surrounds a continuous family of nested periodic orbits. Under these assumptions, the Melnikov function,

$$M(t_0) = \int_{-\infty}^{\infty} \mathbf{g}(\mathbf{z}^*(t),\, t + t_0) \cdot \nabla \tilde{H}(\mathbf{z}^*(t)) dt \tag{13}$$

measures distance between the stable and unstable manifolds of $\mathbf{w}^*$ in the time T-stroboscopic Poincaré section phase plane, where t_0 parameterizes the unperturbed homoclinic orbit $\mathbf{z}^*$. The Melnikov function $M(t_0)$ is proportional to distance between stable and unstable manifolds of $\mathbf{w}^*$ at $\mathbf{z}^*(-t_0)$. Under the above assumptions, the result is that existence of a zero, (a t_0 such that $M(t_0) = 0$), which is simple, $((\partial M/\partial t)|_{t_0} \neq 0)$, implies that the dynamical system Eq. (10) has a transverse homoclinic point and hence possess an embedded horseshoe.

We will choose the square root of eccentricity, $e = \varepsilon^2$, as the small parameter of our system in Eqs. (10),

$$b = \sqrt{1 - \varepsilon}\,. \tag{14}$$

We find the following (noncanonical change of variables) shift of the canonical position q to be convenient,

$$Q = \omega t + q\,. \tag{15}$$

With these change of variables, and Taylor expanding to just first-order terms in ε of Eqs. (10), we find,

$$\begin{pmatrix} \frac{dQ}{dt} \\ \frac{dp}{dt} \end{pmatrix} = \begin{pmatrix} \frac{p}{m} \\ -mg\,\cos(Q) \end{pmatrix} + \varepsilon \begin{pmatrix} \left(\frac{p}{m} - \omega\right)\cos^2(Q - \omega t) + \frac{1}{2}\omega \\ \frac{1}{2} mg\,\cos(\omega t)\cos(Q - \omega t) + \frac{1}{2}\frac{p(p - 2\omega m)\sin(2Q - 2\omega t)}{m} \end{pmatrix} + O(\varepsilon^2)\,. \tag{16}$$

Hence, our autonomous vector field is,

$$\left\langle \frac{p}{m},\, -mg\,\cos(Q) \right\rangle^t, \tag{17}$$

from the zeroth-order Hamiltonian,

$$\tilde{H}(Q, p) = \frac{1}{2}\frac{p^2}{m} + mg\,\sin\,Q\,, \tag{18}$$

which we see is equivalent to the well known full nonlinear pendulum [Goldstein, 1980]. It is easy to find the path of the unperturbed homoclinic orbit through phase space to be given by the equation,

$$p^*_{\pm}(Q) = \pm m\sqrt{2g(1 - \sin(Q))}\,. \tag{19}$$

See Fig. 2. The time-periodic perturbation is,

$$\mathbf{g}(Q, p, t) = \left\langle \left(\frac{p}{m} - \omega\right)\cos^2(Q - \omega t) + \frac{1}{2}\omega, \right. \\ \frac{1}{2} mg\,\cos(\omega t)\cos(Q - \omega t) \\ \left. + \frac{1}{2}\frac{p(p - 2\omega m)\sin(2Q - 2\omega t)}{m} \right\rangle^t. \tag{20}$$

Considering the homoclinic connection orbit of this autonomous system (Fig. 2), Melnikov's method allows us to consider changes to the stable and unstable manifolds as ω and g are varied.

Substitution of $\nabla \tilde{H}(\mathbf{z}^*) = \langle mg\,\cos(Q), p^*/m \rangle$, and Eq. (20) for $\mathbf{g}(\mathbf{z}^*)$, into the Melnikov function

Eq. (13) gives,

$$M_\omega(t_0) = \int_{t=-\infty}^{t=\infty} \left(\left(\frac{p^*}{m} - \omega \right) \cos^2(Q - \omega(t+t_0)) + \frac{\omega}{2} \right) mg \cos(Q) + \left(1/2\, p^* g \cos(\omega(t+t_0)) \cos(-Q + \omega(t+t_0)) + \frac{p^{*2}(p^* - 2\omega m) \sin(2Q - 2\omega(t+t_0))}{2m^2} \right) dt. \tag{21}$$

Using the homoclinic orbit Eq. (19), $\mathbf{z}^*_\pm = \langle Q, p^*(Q) \rangle = \langle Q, \pm m\sqrt{2g(1-\sin(Q))} \rangle$ with a change of variables,

$$dt = \frac{dQ}{\dot{Q}} = \frac{m}{p^*} dQ\,, \tag{22}$$

on the homoclinic orbit changes limits of integration from time integration of $-\infty < t < \infty$ to spatial integration $-(3\pi/2) < Q < \pi/2$. We define $t = 0$ to correspond to a position $Q = -(\pi/2)$ in the "middle" of the separatrix and at other arbitrary times t in the integral Eq. (21), we use the substitution,

$$\begin{aligned} t &= \int_0^t dt = \int_{\frac{-\pi}{2}}^{Q} \frac{dQ}{\dot{Q}} \\ &= \int_{\frac{-\pi}{2}}^{Q} \frac{dQ}{\sqrt{2g(1-\sin Q)}} \\ &= \frac{(\cos Q + \sin Q - 1)\sqrt{1+\cos Q}\, \operatorname{arctanh} \dfrac{\cos Q + \sin Q + 1}{2\sqrt{1+\cos Q}}}{\sin Q \sqrt{2g(1-\sin Q)}}\,, \end{aligned} \tag{23}$$

in,

$$M_\omega(t_0) = \int_{\frac{-3\pi}{2}}^{\frac{\pi}{2}} \nabla \tilde{H}(\mathbf{z}^*) \cdot \mathbf{g}(\mathbf{z}^*, t+t_0) \frac{m}{p^*(Q)} dQ\,. \tag{24}$$

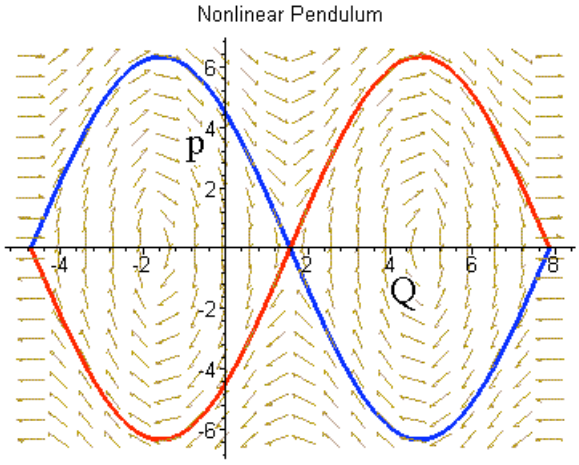

Fig. 2. Homoclinic orbit of zeroth-order autonomous system, Eq. (17), due to zero eccentricity.

Melnikov integrals are generally nontrivial to evaluate, and we resort here to numerical evaluation. The difficulty is due to an infinity of oscillations of the integrand in the finite space, $-3\pi/2 \le Q \le \pi/2$, which should be expected since the integrand is a description of a homoclinic tangle. This particular example allows us to perform a rigorous numerical analysis to evaluate this improper integral. A transverse homoclinic point occurs when $M_\omega(t_0)$ has a simple zero. Since $M_\omega(t_0)$ is continuous and periodic, we consider a homoclinic bifurcation diagram in parameter ω based on the value of the function,

$$C(\omega) = \min_{t_0} |M_\omega(t_0)|\,. \tag{25}$$

We conclude the existence of a simple zero for ω satisfying $C(\omega) = 0$. We find that $C(\omega) = 0$ for all ω, and hence we do not include here a graph of this constant-zero graph. The conclusion however is interesting: there exists a horseshoe for all ω, for all nonzero ε.

While the Melnikov analysis is one of the few tools available in dynamical systems theory which

can be used to prove the existence of an embedded horseshoe for a differential equation (when the unperturbed homoclinic orbit is available), its results are nonetheless often over stated. Smale's theorem [Smale, 1965] states that a transverse homoclinic point implies an embedded horseshoe, of the nth iterate of the map, for some $n > 0$. It is not uncommon that n might be large, indicating a very "slow chaos." In other words, it is possible that on short time scales, the process might seem rather simple and ordered, and only on long time scales do fully developed chaos become evident [Bollt, 1999]. Furthermore, a horseshoe is topologically a Cantor set, and it is not uncommon that such sets might have measure zero. The hope is that we have shown chaos on a set, while perhaps a small set, which is typical. On the other hand, in the presence of resonance layers, separated by KAM-like invariant circles [Meiss, 1992], it is possible to have a layer of highly confined chaos. Finally, our results based on Melnikov analysis are only good for $\varepsilon \ll 1$. In the next section, we numerically investigate such issues.

4. Poincaré Section, KAM and Confined Chaos

We have shown in the previous section that there is a subset of phase space on which Eq. (10)

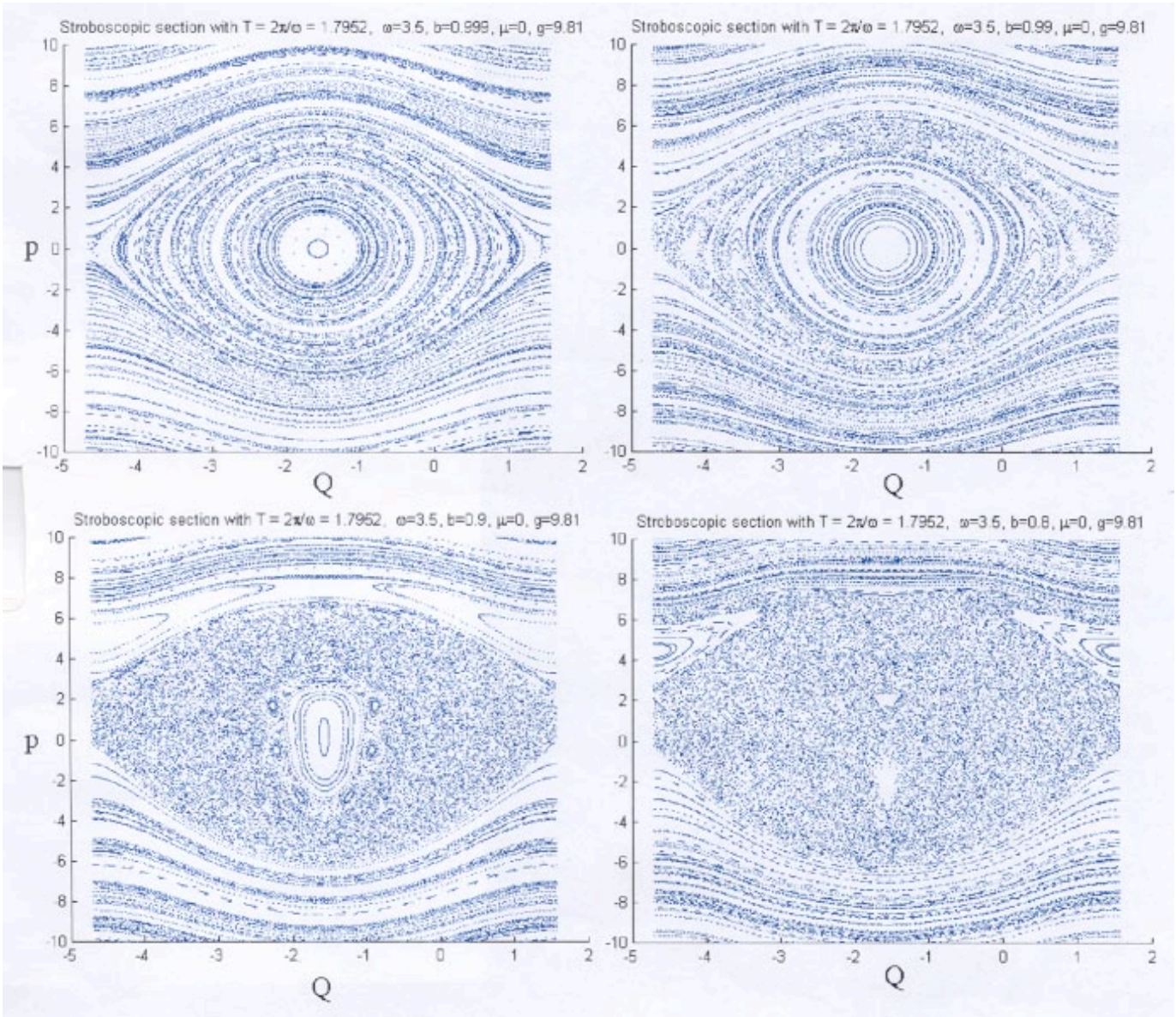

Fig. 3. Stroboscopic Poincaré sections of ETT, Eq. (10), yielding an area preserving map with familiar KAM-like invariant curves with island-around-island resonance regions which separate chaotic "seas." Shown are the parameter values $b = \{0.999, 0.99, 0.9, 0.8\}$ for fixed $\omega = 3.5$.

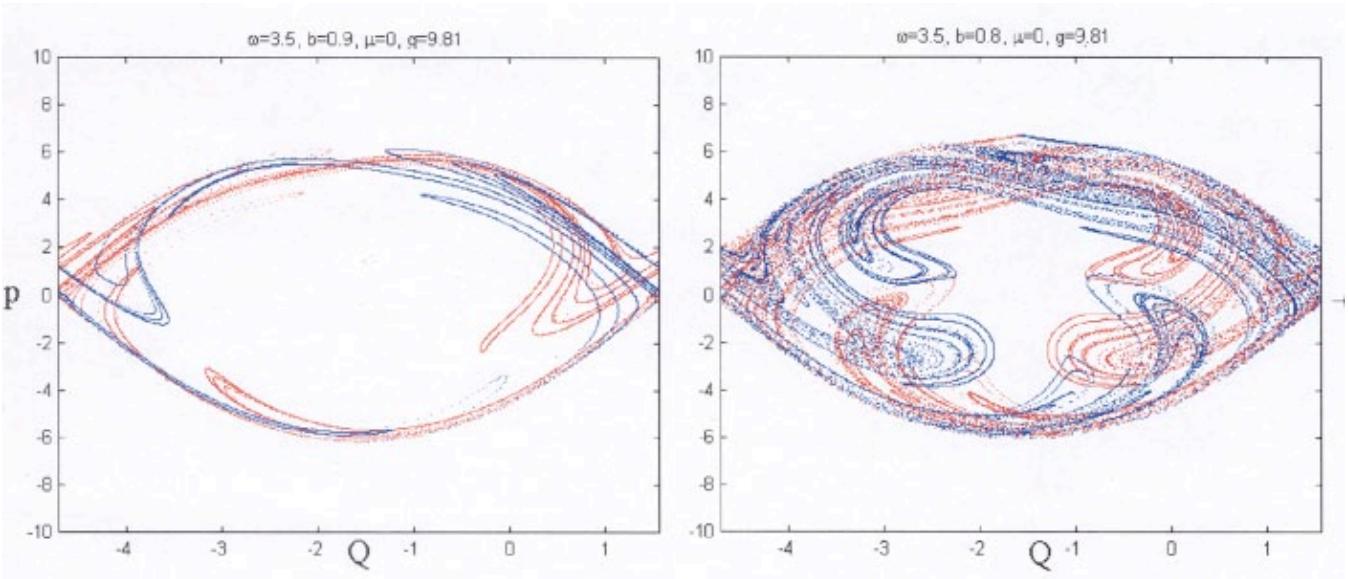

Fig. 4. The homoclinic tangle of stable and unstable manifolds of the fixed point on stroboscopic Poincaré section of ETT, Eq. (10), for parameter values $b = 0.9$, 0.8 and $\omega = 3.5$, comparable to Fig. 3.

displays horseshoe chaos. In this section, we numerically study the area preserving map which is expected of the stroboscopic Poincaré map. See Fig. 3. We observe the expected KAM-like invariant circles [Meiss, 1992], and the familiar path to complexity due to disappearing circles as the parameter b is decreased for a fixed ω. Decreasing b brings us outside of the small ε regime where the above Melnikov analysis was valid. We also observe numerically that while there may be the horseshoes indicated by the Melnikov analysis for small ε, numerically computed homoclinic tangles due to transverse intersection of stable and unstable manifolds can be numerically confirmed for the elliptic case which are not vanishingly small. See Fig. 4.

Consider in Fig. 3 a panel of phase portraits for a path through parameter space of decreasing b, $b = \{0.999, 0.99, 0.9, 0.8\}$ (ε is initially small and increases by Eq. (14)) for fixed $\omega = 3.5$. Observe that as b decreases (ε increases), a familiar island-around-island picture emerges; there is the typical mixed phase space of stable periodic orbits, and quasiperiodic invariant circle "islands", embedded in a bounded Cantor-like chaotic "sea" generated by heteroclinic tangles which emerge from various higher ordered periodicities. As invariant circles are destroyed, more heteroclinic connections are expected to occur between once separated resonances, through the cantori partial-barriers [Meiss, 1992]. The Melnikov analysis performed in the last section is only valid for the main resonance due to the homoclinic connection of the fixed points chosen. The analysis could have equally been applied to any other resonance by replacing the path of integration in Eq. (21) from the fixed points' homoclinic connection, to that of some higher ordered resonance.

Although ε is too large in Fig. 3 for the Melnikov results to apply, we do numerically observe chaos, and in fact the chaotic seas between the island-around-island resonance layers apparently increase in measure with b. Our numerical exploration indicates that such results are general for other parameter paths. As a rule, small ω or small ε tends to correspond to a smaller chaotic sea for those values of ε for which the above Melnikov analysis allows chaos.

Finally in this section we display in Fig. 4 the numerically computed homoclinic tangle of the hyperbolic fixed point responsible for the main connected chaotic component. Compare with Fig. 3.

5. Models 1b and 1c: ETT with Rolling Resistance and Then Moment of Inertia

5.1. *Model 1b: Elliptical tube toy with rolling resistance*

We now add friction to the basic model for Elliptical Tube Toy (ETT). We develop the equations of motion for a bead constrained to move

on an elliptical wire with friction. We follow the generalized force formulation of Lagrange's equations [Goldstein, 1980],

$$Q_j = \frac{d}{dt}\left(\frac{\partial T}{\partial \dot{q}_j}\right) - \frac{\partial T}{\partial q_j}\,. \tag{26}$$

We define all relevant vectors in the force diagram Fig. 5. We assume a friction force of the form,

$$\mathbf{F}_{\rm fric} = -\mu N \frac{\mathbf{v}_\theta}{\|\mathbf{v}_\theta\|}, \text{ where } N = |\mathbf{F}_{\rm grav}\cdot\hat{\mathbf{n}}|\,. \tag{27}$$

In our rotating coordinate frame we have,

$$\mathbf{F}_{\rm grav} = -mg\hat{\mathbf{j}} = -mg(\sin\Omega\hat{\mathbf{e}}_x + \cos\Omega\hat{\mathbf{e}}_y)\,, \tag{28}$$

and,

$$\hat{\mathbf{n}} = \frac{\dot\theta b\cos\theta\hat{\mathbf{e}}_x + \dot\theta\sin\theta\hat{\mathbf{e}}_y}{\|\mathbf{v}_\theta\|}\,, \tag{29}$$

where $\|\mathbf{v}_\theta\| = \sqrt{\dot\theta^2(\sin^2\theta + b^2\cos^2\theta)}\,.$

Therefore,

$$\mathbf{F}_{\rm fric} = \frac{-\mu mg\,\mathrm{sgn}(\dot\theta)|b\cos\theta\sin\Omega + \cos\Omega\sin\theta|}{\sin^2\theta + b^2\cos^2\theta} \times(-\sin\theta\hat{\mathbf{e}}_x + b\cos\theta\hat{\mathbf{e}}_y)\,, \tag{30}$$

and recalling that $\mathbf{r} = \cos\theta\hat{\mathbf{e}}_x + b\sin\theta\hat{\mathbf{e}}_y$, the generalized friction force is,

$$Q_{\rm fric} = \mathbf{F}_{\rm fric}\cdot\frac{\partial\mathbf{r}}{\partial\theta} = -\mu mg\,\mathrm{sgn}(\dot\theta)|b\cos\theta\sin\Omega + \cos\Omega\sin\theta|\,. \tag{31}$$

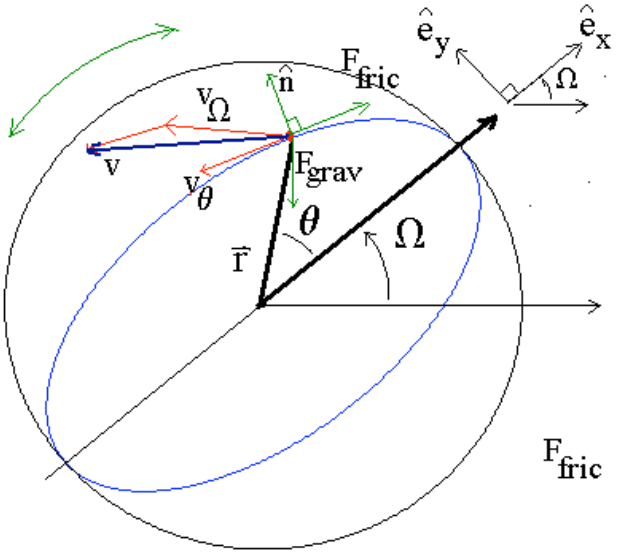

Fig. 5. Schematic drawing defining variables for a bead on a rotating ellipse including forces, with friction.

We get the generalized force due to gravity,

$$Q_{\rm grav} = \mathbf{F}_{\rm grav}\cdot\frac{\partial\mathbf{r}}{\partial\theta} = mg(\sin\Omega\sin\theta - b\cos\Omega\cos\theta)\,. \tag{32}$$

To derive kinetic energy let,

$$\mathbf{v}_\theta = \dot\theta\frac{\partial\mathbf{r}}{\partial\theta} = \dot\theta(-\sin\theta\hat{\mathbf{e}}_x + b\cos\theta\hat{\mathbf{e}}_y) \tag{33}$$

and, $\mathbf{v}_\Omega = \dot\Omega\mathbf{r}_\perp\,.$

Now using $\mathbf{v} = \mathbf{v}_\theta + \mathbf{v}_\Omega$, we find the kinetic energy to be,

$$T = \frac{1}{2}m\mathbf{v}\cdot\mathbf{v} = \frac{m}{2}[(b\dot\Omega - \dot\theta)^2\sin^2\theta + (b\dot\theta - \dot\Omega)^2\cos^2\theta]\,. \tag{34}$$

Hence, Lagrange's equations, Eq. (26) gives,

$$\ddot\theta(\sin^2\theta + b^2\cos^2\theta) - b\ddot\Omega + \dot\theta\sin 2\theta(1-b^2) - \frac{1-b^2}{2}(\dot\theta^2 - \dot\Omega^2)\sin 2\theta = g[(\sin\Omega\sin\theta - b\cos\Omega\cos\theta) - \mu\,\mathrm{sgn}(\dot\theta)|b\cos\theta\sin\Omega + \cos\Omega\sin\theta]\,. \tag{35}$$

It can be verified that that in the limit $\mu \to 0$, we can recover the frictionless system modeled by Eqs. (10).

The generalization of KAM-like invariant circles and other Mather sets due to area preserving twist maps, in which a slight dissipative has been added, is addressed by the Birkoff attractor theory [Arrowsmith & Place, 1990]. These results are numerous, and we summarize a few. No more than one rotational invariant circle can survive in the presence of even a small amount of dissipation. Also the structurally unstable elliptic periodic points at the centers of island chains tend to become either stable or unstable rotational sinks or sources. On the other hand, structural stability of hyperbolic sets [Wiggins, 1990; Arrowsmith & Place, 1990] assures that hyperbolic saddle periodic points persist for a range of small enough dissipation, $\mu < \mu_c$, and likewise other hyperbolic sets, such as embedded horseshoes due to the topology of transversal homoclinic or heteroclinic intersection, as depicted in Fig. 4, also persist for an open set of $\mu \in (-\mu_c, \mu_c)$.

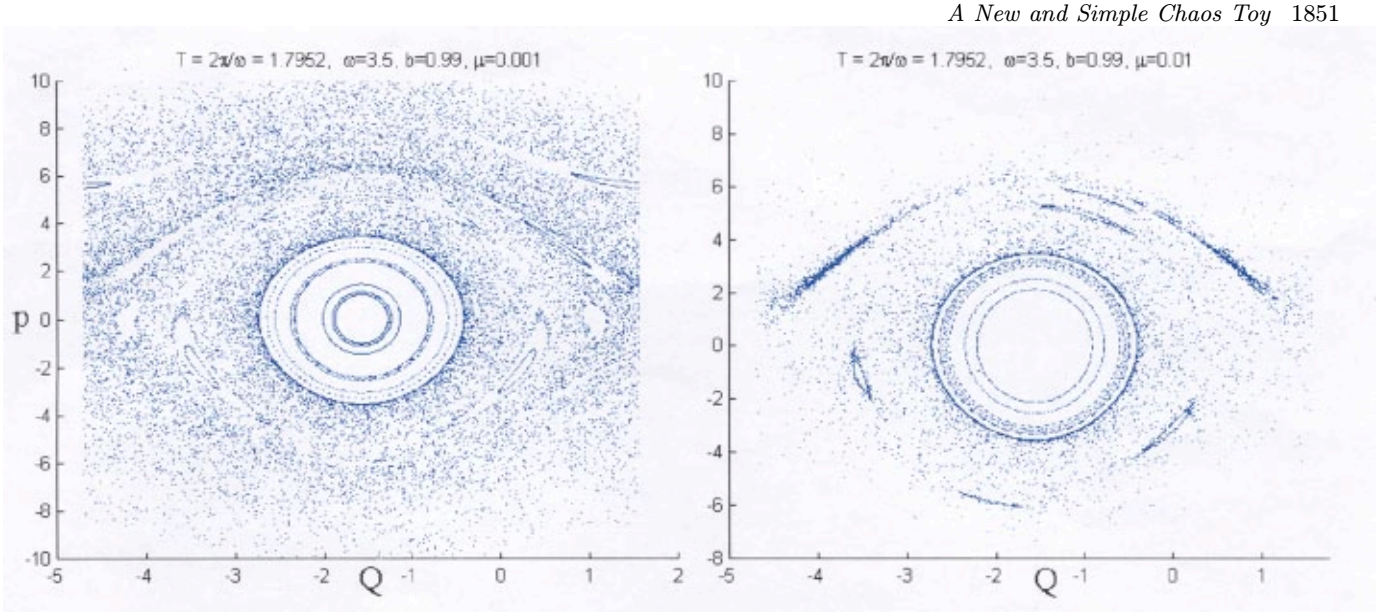

Fig. 6. Even a small amount of dissipation destroys most invariant circles, and changes elliptic fixed points at the center of island chains to rotational sinks or sources. These two phase portraits have small values of friction, $\mu = 0.001,\ 0.01$ respectively, and otherwise match parameter values for the slightly chaotic, almost circular track experiment shown in Fig. 3(b).

Numerically, we find that increasing dissipation destroys most invariant circles, and apparently changes elliptic fixed points at the center of island chains to rotational sinks or sources. See Fig. 6 for two small values of friction $\mu = 0.001,\ 0.01$, and compare to otherwise matching parameter values depicted in Fig. 3(b).

5.2. *Elliptical tube toy ETT with moment of inertia*

In Secs. 2 and 5.1, we derived models for ETT modeled as a bead on a wire, with and without friction respectively. It is not difficult to add the additionally modeling complexity of rolling moment of inertia, without dissipation. We briefly describe the derivation here.

We now allow a and b to be the length of the major and minor axes respectively. Consider a ball bearing of radius r rolling in Fig. 1, in place of the moving bead. Equation (2) is replaced with the center of ball bearing mass position,

$$\mathbf{P}_{\rm cm} = (a-r)\cos(\theta)\hat{\mathbf{e}}_{\mathbf{x}} + (b-r)\sin(\theta)\hat{\mathbf{e}}_{\mathbf{y}}\,, \quad (36)$$

due to an effectively reduced in size ellipse to one of major and minor axes of $(a-r)$ and $(b-r)$, respectively. Velocity is analogous to Eq. (3) and is found by differentiation. The total kinetic energy has the added rotational term, which is $T_{\rm rot} = (I/2)\omega^2$, where $I = (2/5)mr^2$ is the moment of inertia for a solid ball of mass m, and for our system, the nontrivial new derivation is,

$$\omega = \frac{|\dot\theta|\sqrt{(a-r)^2\sin^2\theta + (b-r)\cos^2\theta}}{r}\,, \quad (37)$$

is easily understood by modifying Eq. (33) to allow for major and minor axes of $(a-r)$ and $(b-r)$, and solving the equation $\omega r = \|\mathbf{v}_\theta\|$. Now we can write the total kinetic energy,

$$\begin{aligned} T = T_{\rm cm} + T_{\rm rot} &= \frac{m}{2}\mathbf{v}_{\rm cm}\cdot\mathbf{v}_{\rm cm} + \frac{I}{2}\omega^2 \\ &= \frac{m}{2}\sin^2\theta[(a-r)\dot\theta + (b-r)\dot\Omega]^2 \\ &\quad + \frac{m}{2}\cos^2\theta[(a-r)\dot\Omega + (b-r)\dot\theta]^2 \\ &\quad + \frac{m}{2}[(a-r)^2\sin^2\theta + (b-r)^2\cos^2\theta]\dot\theta^2\,, \end{aligned} \quad (38)$$

and potential energy is analogous to Eq. (5), but due to a shortened ellipse,

$$\begin{aligned} U = mg[&(a-r)\sin\,\Omega\,\cos\,\theta \\ &+ (b-r)\cos\,\Omega\,\sin\,\theta]\,. \end{aligned} \quad (39)$$

The Lagrangian is $L = T - U$, and the steps to find equations of motion are routine.

6. Physical Realization of ETT

We have built a cheap physical rendition of ETT, which we describe briefly here. The elliptical tube was routed into a sheet of wood, with a large enough circular head router so that a teflon ball bearing can roll freely in the track. Then we secured a piece of plexi-glass to the open face to confine the ball to roll in the track, and to provide easy observation. Then we mounted the sheet of wood to a bicycle wheel, center of the ellipse cut to exactly the size of the wheel hub for a secure fit. Then we mounted the wheel with wood to a plane incliner to allow for an effectively adjustable gravity constant. See a photograph of our apparatus shown in Fig. 7. The experiment was obviously very inexpensive, especially since we used only spare parts.

We also include pictures of a few simulated runs of the ETT with friction for comparision to the physical experiment. In Fig. 9, we show a short simulated run of ETT, which we see well matches the character of the physical experiment shown in Fig. 7. It is interesting to note that as in the experiment, there are close recurrences which are followed by separation. A longer run shown in Fig. 10 of the same numerical experiment, with the same initial conditions and parameter settings as in Fig. 9 reveals a signature motion typical of ETT: the ball tends to make seemingly sudden and seemingly random changes of direction. The explanation is simple: the eye is fooled to believe that the ball is rolling on a round track, and that the ball will continue along the corresponding intuitive arc, but due to the ellipse whose orientation is continually changing relative to the constant gravity field, the resulting motion is at first surprising and nonintuitive. We have archived a video of the experiment at: http://mathweb.mathsci.usna.edu/faculty/bolltem/ and at the mirror site: http://www.clarkson.edu/~embollt.

Fig. 7. Photograph of a physical model of ETT, built on a bicycle wheel, and a mounted piece of wood in which was routed the elliptical track. The white teflon ball shown moves freely and chaotically within the elliptical track. This wheel assembly is mounted on an inclining arm so that the effective strength of the gravity constant becomes $g \sin \alpha$, where α is the angle at which the wheel is inclined from horizontal. $\alpha = 90^\circ$ is shown in this picture.

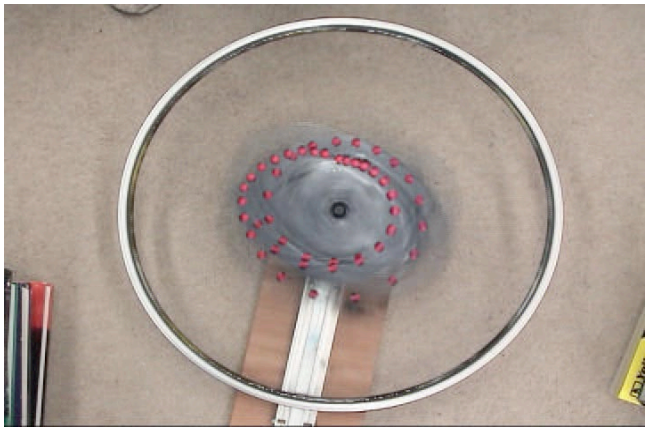

Fig. 8. Motion study photograph of a physical model of ETT. The pink teflon ball is shown in motion by 70 layered still shots, taken at the rate of 15 Hz. An incline of $\alpha \approx 5^\circ$ was shown to control the ball velocity appropriately for the camera used.

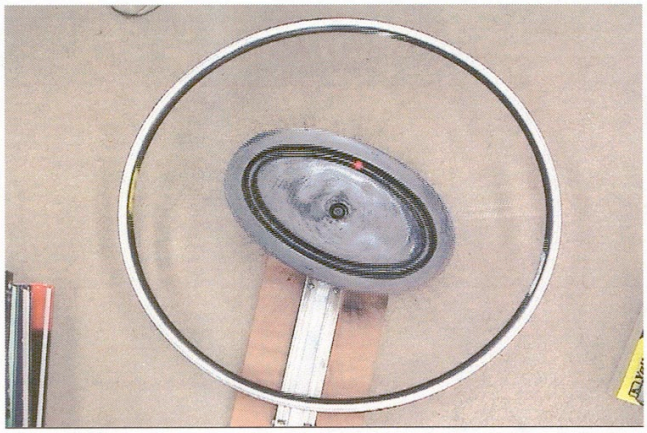

Fig. 9. One of the 70 stills used to create motion study in Fig. 8.

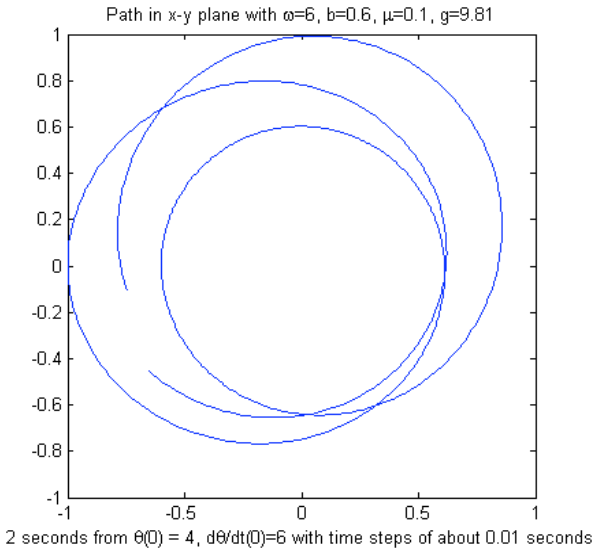

Fig. 10. A short simulated run of ETT, shown in the same physical configuration space as the experiment, which we see well matches the character of the physical experiment shown in Fig. 8. It is interesting to note that as in the experiment, there are close recurrences which are followed by separation.

7. Model 2: Bouncing Tube Toy (BTT)

Now we derive equations of motion for a second example model of a suspended and periodically forced system, which we call, "Bouncing Tube Toy", (BTT). See Fig. 12. The following equations will describe a ball-bearing rolling through an upright circular track, under the influence of a periodic up-and-down drive which effectively periodically alters the magnitude, but not direction, of the gravity force vector. Note that in this model, we do not find that an elliptical track is a necessary ingredient for chaos.

Let R and r be the radii of the track and ball-bearing, respectively. The track oscillates up-and-down cosinuosoidally, $y(t)$ according to Eq. (47). The position and velocity of the center of the ball-bearing are,

$$\mathbf{P}_{\rm cm} = (R-r)\sin\theta\hat{i} + (y-(R-r)\cos\theta)\hat{j}, \qquad (40)$$

$$\mathbf{v}_{\rm cm} = (R-r)\cos\theta\dot{\theta}\hat{i} + (\dot{y}+(R-r)\sin\theta\dot{\theta})\hat{j}\,. \qquad (41)$$

Hence, translational kinetic energy is,

$$T_{\rm cm} = \frac{m}{2}[(R-r)^2\dot{\theta}^2 + 2\dot{y}(R-r)\sin\theta\dot{\theta} + \dot{y}^2]\,. \qquad (42)$$

The rolling kinetic energy of the bearing is,

$$T_{\rm rot} = \frac{I}{2}\omega^2 = \frac{m}{5}(R-r)^2\dot{\theta}^2\,, \qquad (43)$$

since $\omega r = (R-r)\dot{\theta}$ where ω is the angular velocity of a bearing of radius r inside a circle of radius R. The moment of inertia of a solid ball is well known to be, $I_{\rm ball} = \frac{2}{5}mr^2$.

The total kinetic energy T and the potential energy U are respectively,

$$T = \frac{7}{10}m(R-r)^2\dot{\theta}^2 + m(R-r)\sin\theta\dot{y}\dot{\theta} + \frac{1}{2}m\dot{y}^2\,, \qquad (44)$$

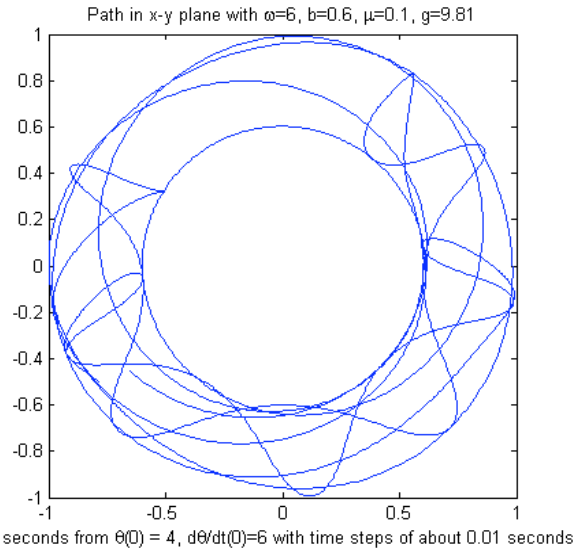

Fig. 11. A longer run of the same numerical experiment, with the same initial conditions and parameter settings as in Fig. 10 reveals a signature motion typical of ETT: the ball tends to make seemingly sudden and seemingly random changes of direction.

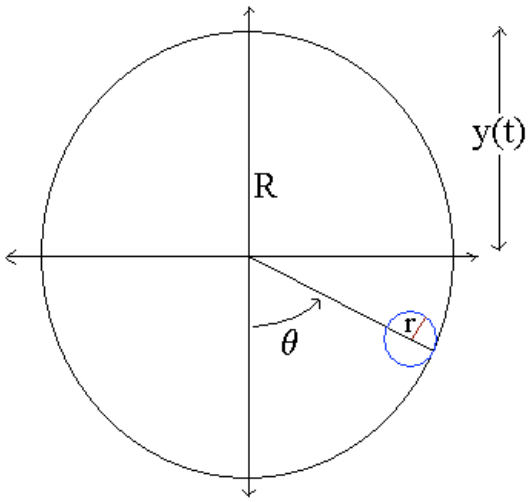

Fig. 12. Schematic drawing defining variables for a ball-bearing on a up-and-down oscillating tubular track.

$$U = mg(y - \cos\,\theta)\,, \tag{45}$$

and the Lagrangian is as usual, $L(\theta,\,\dot\theta,\,t) = T - U$. Again the Lagrangian equations of motion can be found by the second-order equation, $(d/dt)(\partial L/\partial\dot\theta) - (\partial L/\partial\theta) = 0$. We are more interested in the canonical variables to perform a Melnikov analysis.

The Legendre transformation $p = \partial L/\partial\dot\theta$ gives canonical momentum, and the Hamiltonian follows $H(q,\,p,\,t) = \dot q p - L(q,\,\dot q,\,t)$ where we take canonical position to be angle, $q = \theta$.

$$\begin{aligned} H(q,\,p,\,t) = &-\frac{5}{7}\frac{p(-p + mA\dot y\,\sin\,q)}{mA^2} \\ &-\frac{5}{14}\frac{(-p + mA\dot y\,\sin\,q)^2}{mA^2} \\ &+\frac{5}{7}\frac{\dot y\,\sin\,q(-p + mA\dot y\,\sin\,q)}{A} \\ &-\frac{1}{2}m\dot y^2 + mg(y - \cos\,q)\,, \end{aligned} \tag{46}$$

which is nonautonomous due to the drive term, which we will take to be the periodic function,

$$y(t) = B(1 - \cos\,\omega t)\,. \tag{47}$$

For convenience, we have defined $A = R - r$. The canonical equations of motion are

$$\begin{aligned} \frac{dq}{dt} &= H_p = \frac{5}{7}\frac{p - mA\dot y\,\sin\,q}{mA^2}\,, \\ \frac{dp}{dt} &= -H_q = \frac{5}{7}\frac{p\dot y\,\cos\,q}{A} \\ &\quad -\frac{5}{7}\sin\,q\dot y^2 m\,\cos\,q - mg\,\sin\,q\,. \end{aligned} \tag{48}$$

Now to perform the Melnikov analysis described in Sec. 3, we choose the drive amplitude B to be the small parameter which allows use to write the Hamiltonian equations of motion Eq. (48) in the required Melnikov form of Eq. (11). To first-order terms in B, Eq. (48) becomes,

$$\begin{aligned} \begin{pmatrix} \dfrac{dq}{dt} \\ \dfrac{dp}{dt} \end{pmatrix} &= \begin{pmatrix} \dfrac{5}{7}\dfrac{p}{mA^2} \\ -mg\,\sin\,q \end{pmatrix} \\ &\quad + B\begin{pmatrix} -\dfrac{5}{7}\dfrac{\sin\,q\,\sin(\omega t)\omega}{A} \\ \dfrac{5}{7}\dfrac{p\,\cos\,q\,\sin(\omega t)\omega}{A} \end{pmatrix} + O(B^2)\,. \end{aligned} \tag{49}$$

We see that the first-order terms of BTT are closely related to the ETT expansion, in that we again have a system which may be described as a perturbed nonlinear pendulum. This time, the homoclinic connection analogous to Eq. (17) follows the zeroth-order vector field, and we write the gradient of the zeroth-order Hamiltonian

$$\nabla\tilde H(\mathbf{z}^*(t)) = \left\langle mg\,\sin\,q, \frac{5}{7}\frac{p}{mA^2}\right\rangle\,, \tag{50}$$

which is a (phase shifted by $\pi/2$) nonlinear pendulum with Hamiltonian,

$$\tilde H(q,\,p) = \frac{5}{14}\frac{p^2}{mA^2} - mg\,\cos\,q\,. \tag{51}$$

We have a well understood zeroth-order homoclinic orbit, comparable to a phase shifted equation (refhomoc) and Fig. 2,

$$p^*_\pm(q) = \pm\frac{mA\sqrt{70g(1 + \cos\,q)}}{5}\,. \tag{52}$$

Considering the form of the Melnikov integral, Eq. (13) and using the terms of the integrand $\tilde H$ and $\mathbf{g}$ as the zeroth- and first-order terms of expansion Eq. (49), we get

$$\begin{aligned} M(t_0) = &\int_{t=-\infty}^{t=\infty}\frac{25}{49}\frac{\omega(p^*)^2\cos\,q\,\sin\,\omega(t + t_0)}{A^3 m} \\ &-\frac{5}{7}\frac{\omega mg\,\sin^2 q\,\sin\,\omega(t + t_0)}{A}dt \end{aligned} \tag{53}$$

It is easier to deal with a spatial integral on a finite domain with a change in variables, analogous to Eq. (22),

$$dt = \frac{dq}{\dot q} = \frac{7mA^2}{5p^*}dq\,. \tag{54}$$

We have used the zeroth-order homoclinic orbit, Eq. (52). The time limits $-\infty < t < \infty$ changes to the canonical position limits on the homoclinic orbits, $-\pi < q < \pi$. Choosing $t = 0$ to correspond to $q = 0$, and other arbitrary times t can be substituted into Eq. (53) using the derivation,

$$\begin{aligned} t &= \int_0^t dt = \int_0^q \frac{dq}{\dot q} \\ &= \int_0^q \frac{7A}{\sqrt{70g(1 + \cos\,q)}}dq \\ &= \frac{A\sqrt{35}}{5\sqrt{g}}\mathrm{arcsinh}\left(\frac{\sin(q)}{\cos(q) + 1}\right) \end{aligned} \tag{55}$$

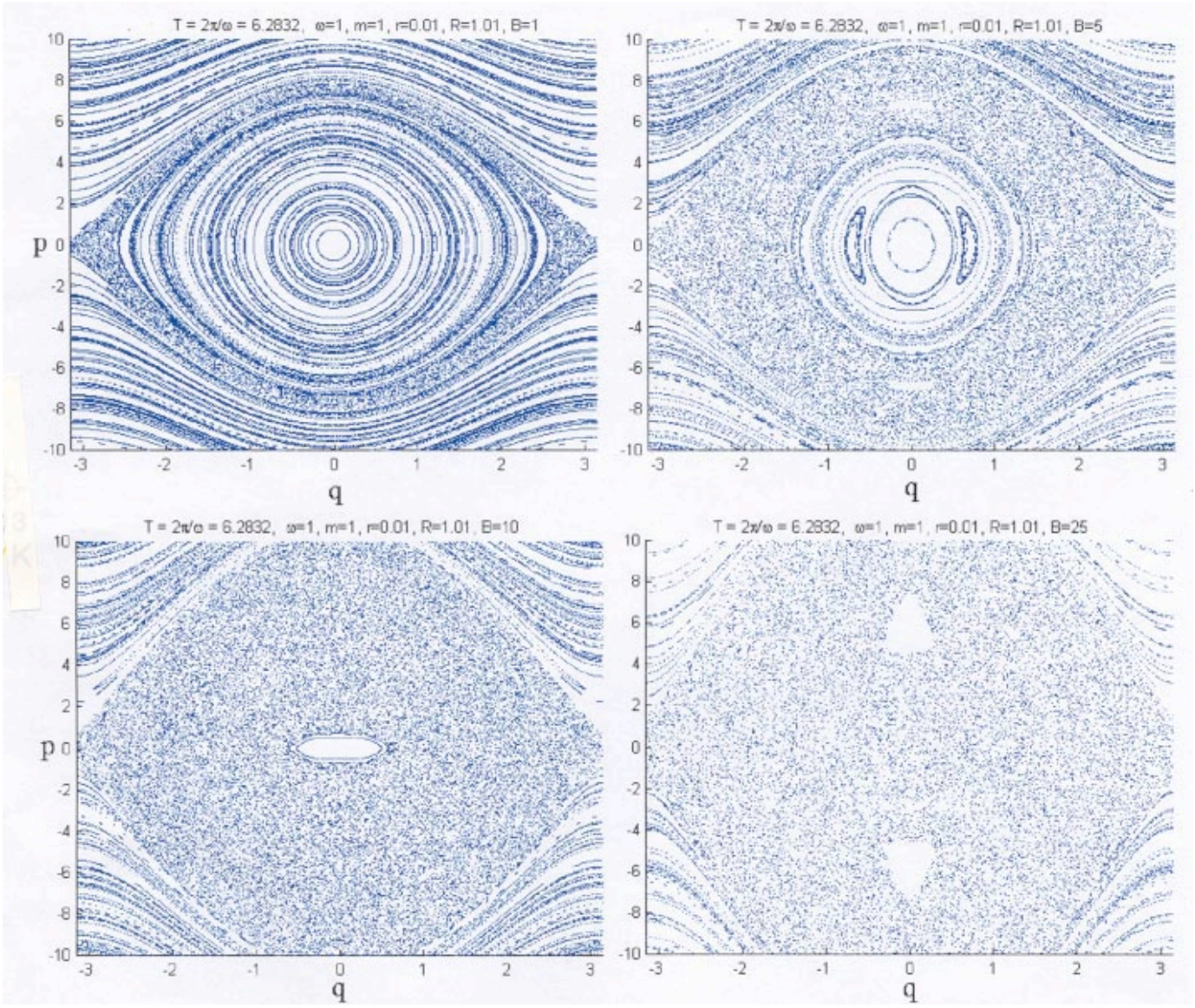

Fig. 13. Stroboscopic Poincaré sections of BTT, Eq. (48), again yielding an area preserving map displaying KAM-like invariant curves with island-around-island resonance regions which separate chaotic "seas." Shown are the parameter values $(m, \omega, R, r) = (1, 1, 1.01, 0.1)$, and we increase through the drive amplitude values $B = \{1, 5\}$.

With substitutions Eqs. (54) and (55), the Melnikov integral Eq. (53) becomes,

$$M(t_0) = \int_{q=-\pi}^{q=\pi} \frac{\omega m g \sqrt{70}(3\cos^2 q + 2\cos q - 1)}{\sqrt{14g(\cos q + 1)}} \times \sin\left[\frac{\omega\left(A\sqrt{35}\,\mathrm{arcsinh}\left(\frac{\sin q}{\cos q + 1}\right) + 5t_0\sqrt{g}\right)}{5\sqrt{g}}\right] dq, \tag{56}$$

which we have again integrated numerically.

Again, as in Sec. 3 in analysis of ETT, we find that $C(\omega) = \min_{t_0} |M_{\pm}(t_0)|$ for all drive frequencies ω, and small amplitude $B \neq 0$. We omit displaying this uninteresting appearing constant zero graph despite its interesting implication. We conclude that for any nonzero small drive amplitude B, we expect an embedded horseshoe.

As further confirmation of the implied chaos, we show in Fig. 13 several phase portraits of the BTT equations (48), on the time T-stroboscopic Poincaré section. Again we see KAM-like invariant circles, which break-up progressively with increasing parameter. Here, we increase drive amplitude B, and observe that resonance layers of confined

chaos become increasingly connected as invariant circles dissappear.

8. Conclusions and Applications

In this paper, we have invented two different models, ETT and BTT, which can both be easily and cheaply built, and which display chaos due to an easily understood mechanism, that of competition between frequencies. We have derived equations of motion based on classical mechanics, and then performed Melnikov analysis, finding that horseshoe chaos is the typical behavior of these systems. But considering the confining role of KAM-like invariant circles to transport in the phase plane for area preserving mappings, we offered that result with caution, since for certain parameter values it could merely mean that there is chaos confined in a region of phase space of trivial measure. We numerically investigate parameter values of these systems outside the validity of the Melnikov analysis, and we found that chaos is probably, and on increasingly nontrivial regions of phase space, as the invariant circle transport barriers are progressively destroyed. We have investigated the role of frictional dissipation on the ETT system, and we note that the most critical set for chaos, a homoclinic tangle, persists under small friction.

Since these systems are easily buildable, and offer themselves to in depth analysis, we consider them to be new and good pedagogical examples of mechanical chaos. We consider them to be more. We are currently pursuing a possible important application for the problem of controlling chaotic oscillations of a crane's cargo during a ship-to-ship transfer of mass at sea, which is a problem of obvious naval importance, [Cranes]. The idea of controlling chaos is to make use of inherent extreme instability naturally built into a chaotic system, so that small control inputs can be used to drastically alter system outputs. A crane problem is essentially a control problem in which a mass is suspended below a support as a pendulum. The essential problem is that "down" is the desirable position neighborhood, for a normally operating crane. It is essentially the nonlinear pendulum depicted in Fig. 2. To make use of chaos control, it would be first necessary to "chaotify" this region of phase space. Following the lessons learned by the models of this paper, we will pursue this by an idea of periodically forcing a suspended pendulum in a track, essentially in a manner equivalent to BTT, where the ball is now a bearing acting as the suspension joint from which we will hang a pendulum arm [Tagg]. This will replace a simply hung pendulum. We expect that such a simple up-and-down forcing of a pendulum arm, together with the circular track in which it can respond will create a situation in which chaos can be "turned-up" for increasing forcing. Then chaos control can be used to stabilize the system [Ott *et al.*, 1990], but in a flexible, and quickly responsive manner. Deliberately engineering instability into a system in this manner has not only proven effective in chaos control [Chen & Dong, 1998], but is the method of choice for example when building highly agile, and adjustable military fighter aircraft. They are built so unstable, that it takes constant computer feedback control to maintain a straight course, but the payback is a responsively controllable aircraft.

Acknowledgments

The authors would like to thank Professor R. Tagg at U. Colorado at Denver Physics Department for helpful discussions. This work was supported by the National Science Foundation under grants DMS-9704639 and DMS-0071314. We would also like to thank Professor Howard Penn, LCDR Joe Skufca, LT Jay Foraker, and Clifford Maxwell for photographic assistance in shooting the physical experiment.

References

Abraham, R. & Marsden, J. E. [1985] *Foundations of Mechanics*, 2nd edition (Perseus Books, Reading MA).

Arrowsmith, D. K. & Place, C. M. [1990] *An Introduction to Dynamical Systems* (Cambridge University Press, NY).

Bollt, E. M. [1999] "Stability of order: Dialing in chaos," *Int. J. Bifurcation and Chaos* **9**(10), 2081–2090.

Chen, G. & Dong, X. [1998] *From Chaos to Order: Perspectives, Methodologies, and Applications* (World Scientific, Singapore).

Cranes: Levine, J., Rouchon, P., Yuan, G., Grebogi, C., Hunt, B., Kostelich, E., Ott, E. & Yorke, J. A., "On the control of US Navy cranes," *Proc. European Control Conf.* (ECC 97), July 1997; Yuan, G., Hunt, B., Grebogi, C., Kostelich, E., Ott, E. & Yorke, J. A. "Design and control of shipboard cranes," *Proc. 16th ASME Biennial Conf. Mechanical Vibration and Noise*, September 1997, Sacramento, CA; see for

example the program of The Advanced Crane Technology Workshop, Norfolk, VA, 1999.

Goldstein, H. [1980] *Classical Mechanics*, 2nd edition (Addison-Wesley, London).

Guckenheimer, J. & Holmes, P. [1983] *Nonlinear Oscillations, Dynamical Systems, and Bifurcations of Vector Fields* (Springer-Verlag, NY).

Lorenz, E. N. [1993] *The Essence of Chaos* (University of Washington Press, Seattle).

Meiss, J. D. [1992] "Symplectic maps, variational principles, and transport," *Rev. Mod. Phys.* **64**, p. 795.

Moon, F. C. [1992] *Chaotic and Fractal Dynamics, An Introduction for Applied Scientists and Engineers*, (John Wiley, NY).

Ott, E., Grebogi, C. & Yorke, J. A. [1990] "Controlling chaos," *Phys. Rev. Lett.* **64**, 1196–1199.

Rott, N. [1970] "A multiple pendulum for the demonstration of non-linear coupling," *J. Appl. Math. Phys.* **21**, 570–582.

Shinbrot, T., Grebogi, C., Wisdom, J. & Yorke, J. A. [1992] "Chaos in a double pendulum," *A. J. Phys.* **60**(6), 491–499.

Smale, S. [1965] "Diffeomorphisms with many periodic points," in *Differential and Combinatorial Topology*, ed. Cairns, S. S. (Princeton University Press, Princeton), pp. 63–80.

Strogatz, S. [1994] *Nonlinear Dynamics and Chaos, With Applications to Physics, Biology, Chemistry, and Engineering* (Addison-Wesley, NY).

Tagg, Project in progress collaborative with R. Tagg and J. Starrett.

Wiggins, S. [1990] *Introduction to Applied Nonlinear Dynamical Systems and Chaos* (Springer, NY).